Magnetic order from molecular oxygen anions

Riyadi, Syarif

Chapter 6

Thin Film Rubidium Oxides and Investigation of Cesium and Potassium Oxides

6.1 Introduction

Among the alkali metal superoxides, the use of KO_2 in breathing apparatus has been well established and widely applied. Potassium superoxide reacts with water and generates oxygen. Otherwise, studies of the synthesis and physical properties of alkali metal oxides have been more fundamental in nature. Not many papers have been published on these materials since the late 80's. The difficulty in chemical synthesis and handling might be the main reason why the alkali metal oxides have not been more widely studied. Even if adequate equipment is present, the handling and synthesis of alkali metal oxides requires patience and much practice.

The bulk physical properties of the alkali superoxides are more or less known. However, the low-temperature crystal structures and their correlation with the magnetic properties are in many cases still poorly understood. For example, the only antiferromagnetic structure studied by neutron diffraction is KO_2 [1]. The 1989 review of Hesse et al. [2] remains a comprehensive overview of most of what is known about alkali oxides. Little further experimental work has been carried out in the two decades since then except for studies of the structural and magnetic properties of the mixed peroxide-superoxide compounds rubidium sesquioxide (Rb_4O_6) [3–5] and cesium sesquioxide (Cs_4O_6) [5]. This has motivated recent theoretical work on the interplay between spin, orbital and structural degrees of freedom in alkali superoxides [6–9], which are increasingly being considered in the same way as transition metal compounds with strongly correlated electrons.

Motivated by the recent highlights on the materials referenced above, it is interesting to explore different alkali metal oxide systems to those that form the main focus of this thesis. Mixed-valent alkali oxides, which nominally contain both peroxide and superoxide anions, are of particular interest. Rb_4O_6 and Cs_4O_6 both exhibit spin glass magnetic behavior below 10 K [5], suggesting that their magnetic exchange interactions are weak. One may expect to strengthen the exchange interactions by using denser structures, in which there should be a greater degree of orbital overlap. Three obvious approaches towards obtaining denser structures are to apply external pressure, chemical pressure (both on bulk samples), or epitaxial strain (thin film samples). Working with external pressure on air-sensitive alkali oxides promises to be challenging and was neglected from the point of view of time available. However, chemical pressure can readily be applied by the replacement of Rb and Cs with smaller alkali cations. For example, it is currently unclear from the literature whether potassium and sodium sesquioxide exist. If so, their physical properties are entirely unknown. It is quite likely that new and unexplored phases exist, the physical properties of which might give further insight into p-electron magnetism. The effect of epitaxial strain on thin film samples of alkali oxides is unexplored. This chapter is mostly focused on preliminary investigations of thin film rubidium oxides and attempts to explore new phases in the potassium and cesium oxide systems.

6.2 Thin Film Rubidium Oxides

Noticing the different magnetic properties that RbO_x systems can have (Chapters 3 & 4), controlling the oxygen content is the key to complete exploration of the entire phase diagram. In the direct oxidation method applied to bulk samples, intermediate mixing/grinding has to be carried out several times in order to get pure samples. In other words, bulk synthesis often results in inhomogeneous samples and the degree of oxidation is difficult to control. Thin film deposition might allow the oxidation to be more closely controlled and overcome some of the difficulties faced in bulk synthesis.

Several studies have been reported on the deposition and oxidation of thin layers of alkali metals. In the first half of the 20^{th} century Lovell et al. reported attempts to deposit alkali metals on a glass surface by an evaporation method [10, 11]. The deposition was controlled by monitoring the electrical conductivity. This method of deposition is somewhat similar to my first attempts at direct oxidation at high temperature, where a piece of rubidium was evaporated on mild heating and stuck to the glass surface of the reaction flask to form a thin metal mirror. The surface of this rubidium layer turned different colors on exposure to oxygen, suggesting that a rich rubidium oxide (RbO_x) phase diagram can be accessed in thin layers. I therefore attempted to deposit rubidium oxides in the form of thin films by using alkali metal dispensers obtained from SAES Getters.

There are not many reports on thin films of rubidium oxides. The most sys-

tematic study on the oxidation of a rubidium layer is that of Wu et al. [12, 13]. They reported the formation of both peroxide (O_2^{2-}) and superoxide (O_2^-) species during oxidation of rubidium. The sequential formation of O^{2-}, O_2^- and O_2^{2-} has been reported for the oxidation of other alkali metal films [14, 15]. Nevertheless, all of these studies focused only on the different types of oxygen species that can be formed and did not attempt to control the oxygen content. In contrast to the difficulties faced in bulk synthesis, the oxidation of thin films is promising in terms of sample homogeneity and stoichiometry control. In this part of the chapter, the deposition of thin film rubidium oxides is explored as a function of substrate temperature and compared with the phases formed by bulk synthesis.

The (100) plane of single crystal insulating magnesium oxide (MgO) was used here as the substrate. Even though epitaxial growth was not the main intention of this experiment, MgO was chosen because the cubic lattice parameter (4.212 $\mathring{A}$) matches well with that of the basal plane of tetragonal RbO_2. In order to maintain good thermal contact, the substrate was put on top of a stainless steel sample holder and clamped in place using spot-welded thin tantalum wires on both ends. To remove unwanted impurities, the MgO substrate was pre-treated by ultrasonification in technical grade (96%) acetone and ethanol for 15 minutes each. Afterwards, the substrate was subjected to 10^{-6} mbar of O_2 at 650°C for 180 minutes. This treatment removes carbon on the surface of the substrate by the formation of CO_x gas that is later pumped away. Annealing in an O_2 atmosphere was continued during cooling down of the substrate to room temperature.

After annealing, the cleanness of the MgO surface was checked by x-ray photoemission spectroscopy (XPS). As seen in Figure 6.1, no other impurities are present except small traces of carbon. An instrumental offset in energy gave rise to a shift in the spectra. Therefore, the observed binding energies were corrected by using the magnesium $2p$ binding energy (tabulated in the literature as 50.5 eV) as a reference line. Magnesium Auger lines are present between 300 and 400 eV. Oxygen Auger lines around 1000 eV were also observed. Next to the oxygen $1s$ core line, an energy loss line appears at 20-25 eV higher binding energy. This broad line often appears in insulators due to interactions of the photoelectrons with other electrons on the surface of the sample.

Figure 6.2 shows the Rb $3d$ photoemission lines of a rubidium metal film deposited on MgO at 40°C by passing 5.5 A current through the rubidium dispenser; this yields a deposition rate of 0.2 $\mathring{A}$/s. The time of deposition corresponded to a Rb layer of nominal thickness 90 $\mathring{A}$. Due to the air-sensitivity of the sample, ex-situ characterization such as x-ray diffraction could not be performed to determine the structure and thickness of the film. For pure Rb metal, the splitting of the $3d_{3/2}$ and $3d_{5/2}$ lines is reported to be 1.55 eV, with the $3d_{3/2}$ line found at higher energy [16]. Although no obvious spin-orbit splitting is observed for the current sample, the peak is nevertheless best fitted using two profiles consistent with the $3d_{3/2}$ and $3d_{5/2}$ lines. The Rb $3d_{5/2}$ line is present at 111.5 eV, consistent with the literature value [16]. The formation of rubidium oxide phases was previously reported to alter the line shape [12]. The observed spin-orbit splitting for the two-

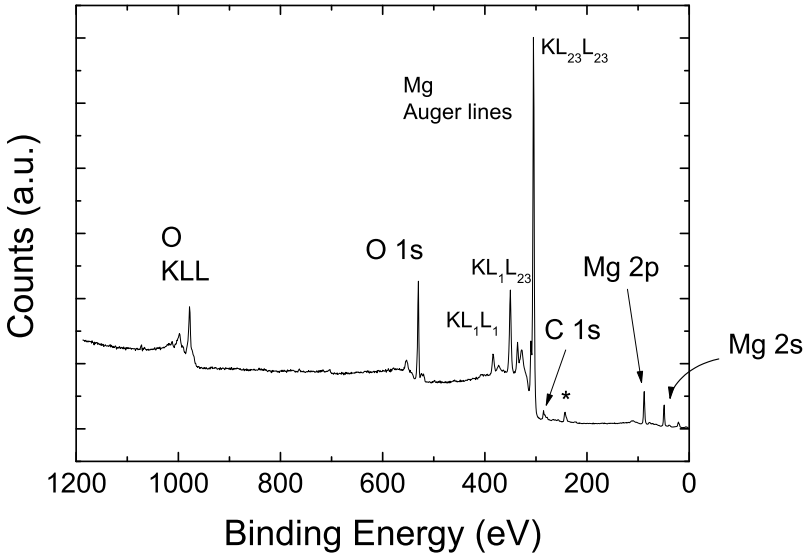

Figure 6.1. X-ray photoemission spectrum of treated MgO substrate. The peak marked with $*$ is suspected to be the Ta (tantalum) $4d$ line (tantalum wire was spot-welded to the stainless-steel sample holder to clamp the MgO substrate in place).

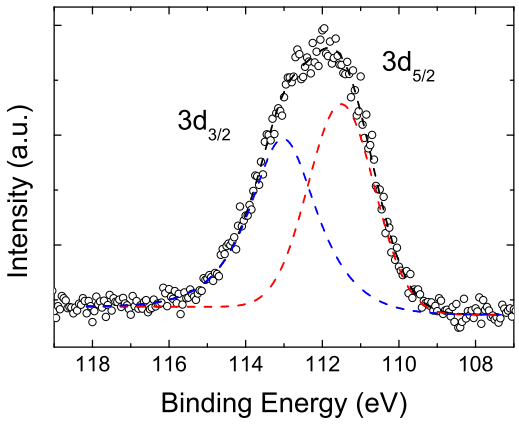

Figure 6.2. Photoemission lines of rubidium on MgO substrate.

peak fit (1.55 eV) is in agreement with the literature value. Mg 2s and 2p lines were also observed in the spectra. This indicates that the incoming x-ray photons penetrate through the rubidium layer and excite photoelectrons from MgO surface. It is possible that island growth occurs or that rubidium is intercalated into interstitial sites in the MgO substrate. It is predicted that island growth is more likely to occur, so that the MgO surface is "seen" by the photons.

Rubidium oxide was deposited on the MgO at the same rate of 0.2 $\mathring{A}$/s but in a background pressure of 10^{-6} mbar oxygen. Deposition was carried out for 10 minutes, corresponding to a nominal film thickness of around 12 nm.

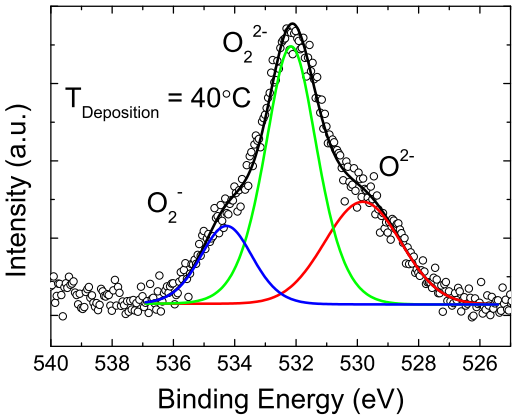

Figure 6.3. Photoemission spectrum around O 1s peaks of rubidium oxides deposited on MgO substrate at 40°C.

Figure 6.3 shows the O 1s lines for rubidium oxide deposited at 40°C. An oxide (O_2^-) line appears close to 530 eV. This suggests the formation of Rb_2O, but a contribution from MgO cannot be ruled out; a weak Mg 2p line is observed at 50 eV, which must come from the substrate. The other two peaks with higher binding energies are assigned to the peroxide (O_2^{2-}) and superoxide (O_2^-) species. The binding energy difference between these two oxygen species is consistent with that reported in the literature for Li, Cs and K oxide films, 2-3 eV [17, 18]. All three peaks were fitted by Pseudo-Voigt profiles with adjustable Gaussian and Lorentzian fractions. The O_2^- line at ~530 eV is broader (2.9 eV) than the O_2^{2-} and O_2^- lines (2.0 eV), consistent with partially overlapping peaks from both MgO and Rb_2O. The integrated intensities of the superoxide and peroxide peaks are in the ratio 1:3. It can be inferred that deposition at 40°C leads to the formation of three different oxygen species: oxide (O^{2-}), peroxide (O_2^{2-}), and superoxide (O_2^-).

Other depositions were conducted at higher substrate temperatures in order to monitor the oxidation of thin film rubidium. Figure 6.4 shows the oxygen 1s

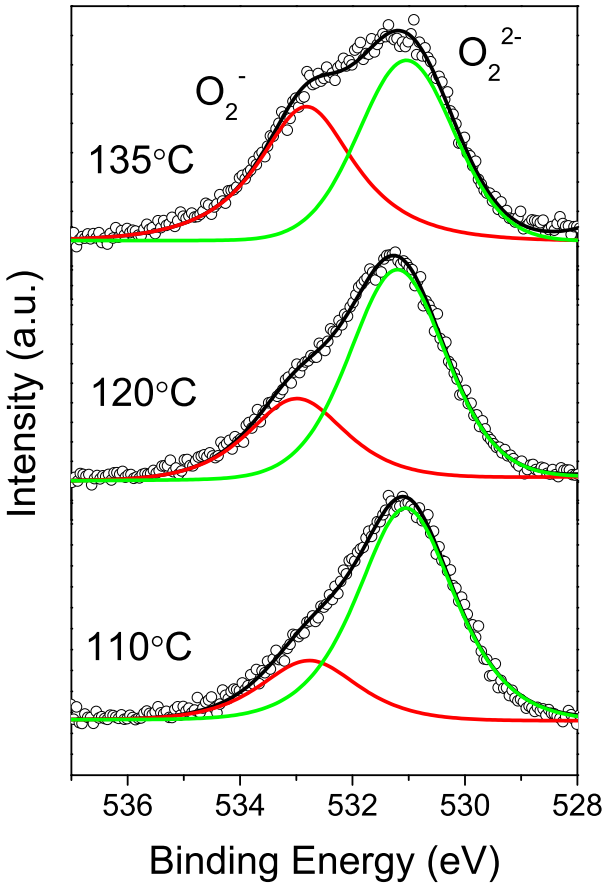

Figure 6.4. Photoemission spectra around oxygen 1*s* peaks for rubidium oxides deposited at different temperatures.

peaks for films deposited at 110°C, 120°C, and 135°C. In each case peroxide and superoxide peaks can be fitted well by single pseudo-Voigt profiles with FWHMs of ∼2.0 eV. Increasing superoxide content with increasing deposition temperature is noticeable in the figure. Both oxygen peaks shift to lower energy with increasing deposition temperature. This feature has previously been observed for oxygen adsorption by rubidium deposited on an InSb substrate [12, 19]. Similarly, the 3d line of rubidium undergoes a continuous shift towards lower binding energy (see Figure 6.5). Other works on thin films of alkali and alkaline-earth metal oxides attribute this binding energy shift to the Madelung potential of the ions [15, 20]. For metallic films, free electrons tend to "screen" incoming photons during the photoemission process. In insulating ionic oxides, the ionic potential from the surrounding environment, i.e. the Madelung potential, has the same effect. This leads to the shift in binding energy observed in x-ray photoemission spectroscopy. With increasing deposition temperature, it appears that more superoxide is formed. The formation of superoxide then affects the electrostatic potential across the film. Based on this argument one can also say that with increasing temperature, the oxidation becomes more uniform, with fewer vacancies and defects. In other words, there is a more uniform distribution of the electrostatic potential. This supports the statement of Wu et al. that the three dimensional formation of RbO_2 and Rb_2O_2 is related to the shift of the binding energy [12]. However, more characterization is needed in order to confirm this speculation. The observed coexistence of superoxide and peroxide might signify the formation of Rb_4O_6, while excess peroxide anions are incorporated in the form of Rb_2O_2. The crystallinity of the films, however, should be investigated.

It is clear from the experiments that the ratio between superoxide and peroxide anions in the films can be tuned by varying the deposition time and substrate temperature. From the initial results, it appears that superoxide is favored by oxidation at higher temperature. Extending the deposition time is likely to result in higher superoxide content. Both issues need to be explored further. At present it is unclear whether homogeneous rubidium oxides are formed or whether RbO_2 and Rb_2O_2 form separate clusters. However, the fact that Rb_4O_6 exists in bulk, as well as the observations that both cubic and tetragonal RbO_{2-x} phases can accommodate a range of oxygen vacancies (see Chapters 3 & 4), suggest that thin film growth may be a convenient way to closely control the oxygen content. The choice of substrate will also likely affect the phases obtained. The substrate used, cubic MgO with a lattice parameter of 4.21 $\mathring{A}$, perfectly matches the lattice parameter of the basal plane of tetragonal RbO_2 and the a lattice parameter of Rb_2O_2. The [001] plane of titanium dioxide (TiO_2) might be a good candidate for a substrate for the epitaxial growth of Rb_4O_6. The basal plane lattice parameter of tetragonal TiO_2 is 4.594 $\mathring{A}$, thus it might be possible to deposit one unit cell of strained Rb_4O_6 ($a \sim 9.3242$ $\mathring{A}$) on top of four unit cells of TiO_2 ($a \sim 9.2$ $\mathring{A}$). The next step in the investigation reported here might be to perform deposition at lower substrate temperature and to study the effects of the substrate cooling rate and oxygen partial pressure. If crystalline 3D films can be deposited on

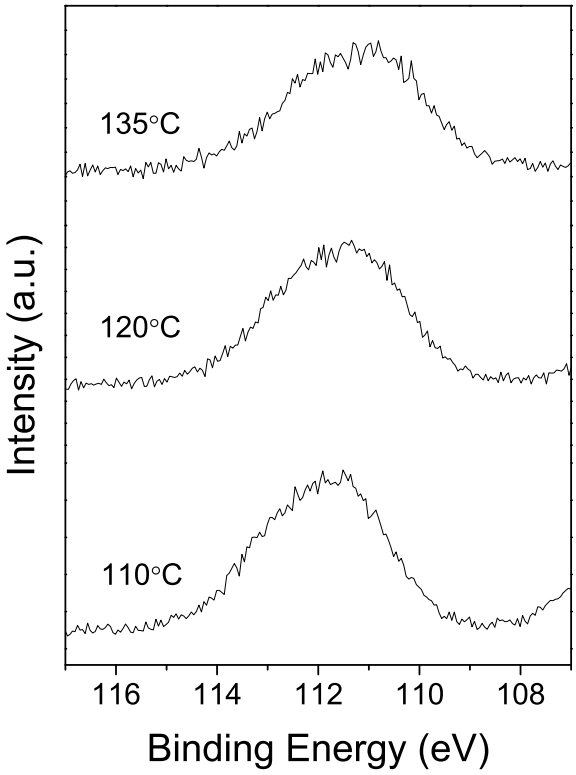

Figure 6.5. Photoemission spectra showing rubidium $3d$ levels in RbO_x thin films deposited at different temperatures.

MgO, it would be interesting to investigate their physical properties. For this it would be necessary to grow a protective capping layer (probably Au) on top of the films so that they can be transferred to other instruments. Structural properties could then be investigated by x-ray diffraction, and the magnetic and transport properties could also be studied.

6.3 Cesium Oxides (CsO_{2-x})

Cesium superoxide (CsO_2) was synthesized by the procedure described in Chapter 5. $CsOH.H_2O$ was unavoidably present as an impurity of a few percent. In contrast to the oxidation of rubidium, intermediate phases with various colors were observed during the oxidation of cesium in liquid ammonia. A brown color appeared after 20 minutes of reaction, which slowly turned to pink before the yellow color of CsO_2 appeared. After liquid ammonia was evaporated from either the brown or pink solution, powders that were dark purple in color were obtained. The crystallinity of these intermediate phases was very poor and the XRD patterns did not correspond to any of the known cesium oxide phases; several phases might coexist in these samples (see Figure 6.6). It appears to be difficult to obtain single phases of these cesium oxides by the solution method. Further annealing in inert atmosphere might improve the purity of such samples, but insufficient time prevented further exploration.

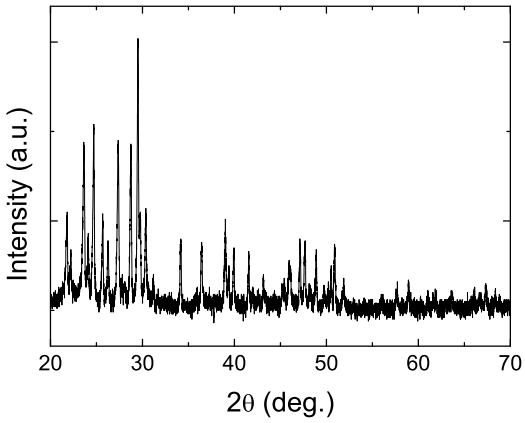

Figure 6.6. XRD pattern of intermediate phase (dark purple) obtained from incomplete oxidation of cesium metal in liquid ammonia.

Attempted thermal decomposition of CsO_2 at 200°C did not give rise to any new phases. Thermal decomposition should be carried out at higher temperatures in order to see whether new phases exist. The synthesis of Cs_4O_6 by the solid state

reaction of CsO_2 and Cs_2O has been reported [5]. "Cubic CsO_2" was identified as an impurity in the XRD pattern of Cs_4O_6; however, CsO_2 is tetragonal at room temperature [2] and this impurity is likely to be a novel CsO_{2-x} phase. More effort should be applied to the exploration of other cesium oxide phases.

6.4 Potassium Oxides (KO_{2-x})

Similar to RbO_2 and CsO_2, potassium superoxide (KO_2) also adopts a tetragonal structure at room temperature. Potassium superoxide with high purity (95%) was obtained from Alfa Aesar chemicals. Attempts to synthesize other KO_x phases were made by thermal decomposition and solid state reaction. Potassium peroxide (K_2O_2) can be easily obtained by thermal decomposition of KO_2 at 300°C for 10 hours. Old reports have claimed the existence of potassium sesquioxide (K_4O_6), which can be synthesized by rapid oxidation in liquid ammonia or by the thermal decomposition of KO_2 [21–23]. Other work also reported the synthesis of K_4O_6 at high temperatures [24], either by the oxidation of K_2O_2 at 560°C or by decomposition of KO_2 at 460°C in a closed quartz ampoule. The color of K_4O_6 has been reported to be brick red [25]. However, there is no firm evidence for the existence of this phase and no sample characterization has ever been reported.

I carried out attempts to synthesize K_4O_6 using the following methods: 1) thermal decomposition of KO_2; 2) solid state reaction of KO_2 and K_2O_2; 3) solid state reaction of KO_2 and K_2O; 4) direct oxidation of potassium metal in ammonia. The thermal decomposition of KO_2 was first followed in a DSC/TGA experiment. The experiment was carried out in a reducing atmosphere (Ar). As seen in Figure 6.7, there are three obvious phase transitions. The first phase transition around 140°C is related with orientational disordering of the superoxide dumbbells to give a cubic structure [26]. Another phase transition occurs at around 320°C along with a weight decrease. This corresponds to the formation of a potassium oxide with oxygen content lower than that of KO_2. Thermal decomposition at 300°C resulted in the formation of potassium peroxide (K_2O_2), while heating at below 300°C did not decompose KO_2. Increasing the temperature to values between 300°C and 370°C always gave only K_2O_2 as the end product. The DSC peak at 370°C corresponds to the melting point of KO_2. Thermal decomposition above the melting point of KO_2 resulted in the formation of a brown/red powder. However, the brown/red color only persisted at high temperature and became yellow on cooling the sample to room temperature. XRD patterns showed equal fractions of tetragonal KO_2 and K_2O_2. X-ray diffraction at high temperature was attempted by sealing the powder in vacuum in a 0.5 mm capillary. However, the oxygen evolution that occurred on heating broke the capillary, instantly decomposing the sample.

The solid state reaction of KO_2 and K_2O_2 was attempted by heating the starting materials at 300°C inside a closed ampoule filled with inert gas (Ar) for 12 hours. XRD showed that no reaction occurred. Annealing at 325°C yielded the

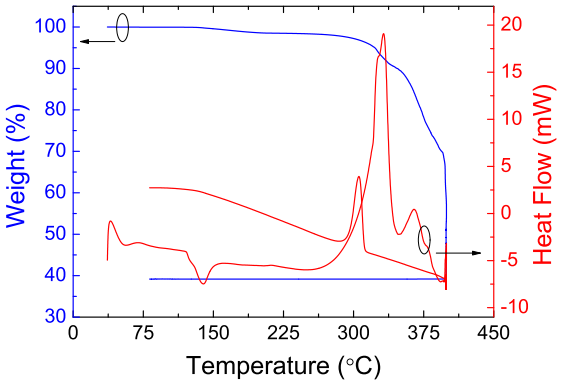

Figure 6.7. DSC/TGA curves of KO_2.

same result. Attempts to synthesize K_4O_6 were also made by using K_2O instead of K_2O_2. However, a mixture of KO_2 and K_2O_2 was again obtained (see Figure 6.8). Despite the lower oxygen content of the K_2O precursor, perhaps annealing allows a stable form of K_2O_2 with oxygen deficiencies to be obtained. This was inferred from the fact that the lattice parameter was smaller by $\sim$0.02 $\mathring{A}$ than that of pure K_2O_2. Oxygen deficiencies might also be incorporated in KO_2. Heating to higher temperature ($>$ 370°C) melted the powder and a colorless material remained in the crucible. Possibly the sample decomposed (oxygen is released), but the phase could not be identified because it reacted with and stuck to the crucible surface. It is inferred that K_4O_6 cannot be synthesized by the solid state reaction method.

Attempts to oxidize potassium in liquid ammonia were also carried out, in similar fashion to experiments involving rubidium and cesium metal. The oxidation of potassium was slower than that of rubidium and cesium. The blue solution turned colorless after 3 hours of oxidation. A further 4-5 hours oxidation was necessary to obtain a yellow solution. White powder was obtained when the reaction was stopped before the yellow solution formed. X-ray powder diffraction revealed that the main phase was K_2O_2 (see Figure 6.9), which was accompanied by another phase that could not be identified (peaks marked by $*$ in Figure 6.9). No other colors were observed during the oxidation, which thus proceeds differently from the oxidation of cesium metal described above. In order to synthesize KO_2, oxidation was carried out until the yellow solution was seen. Afterwards, the liquid ammonia was evaporated. During ammonia evaporation, dry oxygen was passed through the solution. Annealing with oxygen at room temperature was continued on the resulting powder for another 2 hours. The end product was tetragonal KO_2. No indication of the formation of intermediate potassium oxide phases was observed by the liquid ammonia method.

The synthesis of potassium sesquioxide (K_4O_6) was also attempted by direct

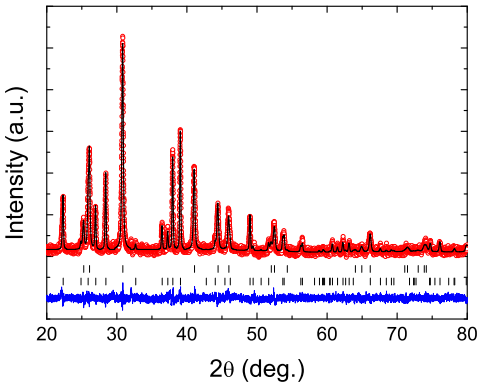

Figure 6.8. XRD pattern of sample obtained from the solid state reaction of KO_2 and K_2O. The pattern shows the phase coexistence of KO_2 and K_2O_2.

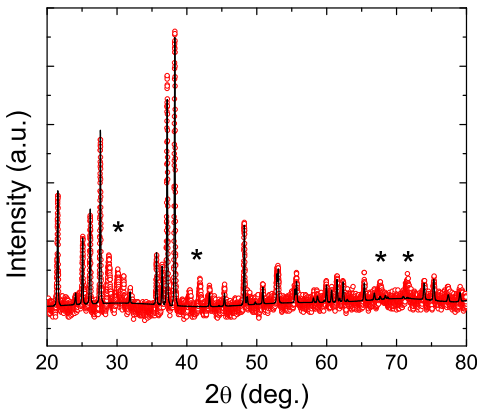

Figure 6.9. X-ray diffraction pattern of the intermediate phase obtained from the oxidation of potassium in liquid ammonia ($*$ = unidentified phase).

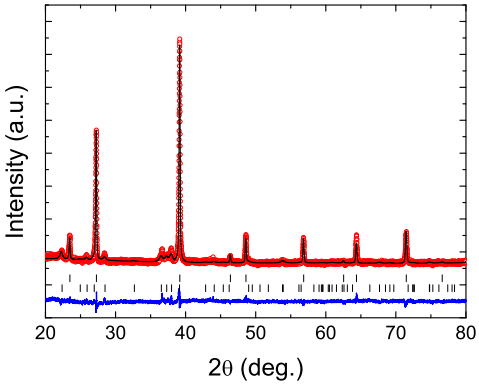

Figure 6.10. XRD pattern of K_2O obtained from direct oxidation of potassium metal at high temperature. The small impurity was identified as K_2O_2.

oxidation of potassium metal (K). Potassium metal was melted inside a round bottomed flask and heated to 200°C. Oxygen was introduced slowly in order to avoid the formation of potassium superoxide (KO_2). A metallic bronze color was seen as soon as the oxygen made contact with the molten metal, probably corresponding to sub-oxides of potassium. Further oxidation resulted in the formation of a powder with a reddish brown color. As was mentioned earlier, homogeneity is the main problem in the synthesis of alkali metal oxides by the direct oxidation method. The sample must be ground and oxidized repeatedly in order to get a homogeneous sample. By careful oxidation and repeated grinding, potassium oxide (K_2O) was obtained (see Figure 6.10). A small impurity was present in the form of potassium peroxide (K_2O_2). Further oxidation resulted in the formation of KO_2. No indication of the formation of K_4O_6 was observed by this synthesis route.

Vannerberg mentioned that it is possible to synthesize potassium oxide with intermediate oxygen content by the oxidation of potassium metal using nitrous oxide (NO) [24]. This was attempted in the same manner as the direct oxidation of potassium metal with oxygen. The reaction was carried out at 200°C inside a round bottomed flask and resulted in the formation of K_2O and another phase that could not be identified. K_2O is a light brown powder, whereas this sample had a dark brown to red color. Looking at the precursors of the reaction, perhaps nitrogen is incorporated in the second phase. The x-ray diffraction pattern of this sample is shown in Figure 6.11. Further reaction of this sample with NO gas gave a white powder that slowly melted and then quickly evaporated within a minute or two. Further investigations are necessary into the reaction of potassium with NO.

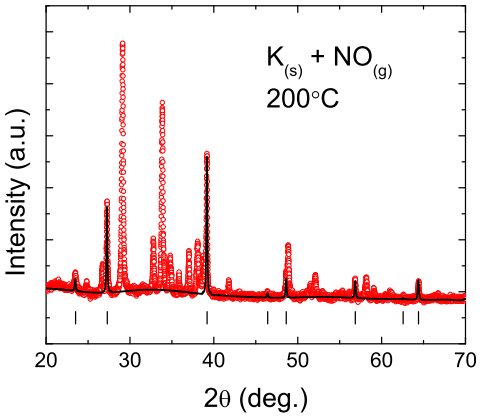

Figure 6.11. The x-ray diffraction pattern of the sample obtained from the reaction of potassium metal (K) with NO (gas) at 200°C. The fit (red line) is to K_2O.

6.5 Conclusions

Thin films of rubidium oxides were deposited on MgO (100) substrates at different temperatures. The formation of different molecular oxygen species was observed by XPS, suggesting a rich phase diagram and the ability to closely control the oxidation state of the molecular oxygen anions. A continuous shift of the O 1*s* and Rb 3*d* lines towards lower binding energy with increasing substrate temperature indicated the increasingly three dimensional nature of the rubidium oxide films. X-ray diffraction should be carried out to characterize the structures of the films; for this, the deposition of a thin capping layer will be necessary.

Attempts to synthesize potassium and cesium oxides with oxygen content lower than AO_2 were carried out using different synthetic methods: direct oxidation at high temperature, oxidation in ammonia solution, and thermal decomposition of the alkali superoxides. The oxidation of potassium in ammonia gave only KO_2, with no intermediate phases. The thermal decomposition of KO_2 always led to the formation of potassium peroxide (K_2O_2). Solid state reactions involving potassium oxides (KO_2 + K_2O_2 and KO_2 + K_2O) were also unsuccessful in synthesizing K_4O_6. However, it is likely that novel phases do exist in the cesium oxide phase diagram; more effort is required to explore it in more detail.

Bibliography

[1] Smith, H. G., Nicklow, R. M., Raubenheimer, L. J., and Wilkinson, M. K. *J. Appl. Phys.* **37**, 1047 (1966).

[2] Hesse, W., Jansen, M., and Schnick, W. *Prog. Solid State Ch.* **19**, 47 (1989).

[3] Jansen, M. and Korber, N. *Z. Anorg. Allg. Chem.* **598**, 163 (1991).

[4] Jansen, M., Hagenmayer, R., and Korber, N. *CR Acad. Sci. II C* **2**, 591 (1999).

[5] Winterlik, J., Fecher, G. H., Jenkins, C. A., Medvedev, S., Felser, C., Kuebler, J., Muehle, C., Doll, K., Jansen, M., Palasyuk, T., Trojan, I., Eremets, M. I., and Emmerling, F. *Phys. Rev. B* **79**, 214410 (2009).

[6] Kovacik, R. and Ederer, C. *Phys. Rev. B* **80**, 140411(R) (2009).

[7] Ylvisaker, E. R., Singh, R. R. P., and Pickett, W. E. *Phys. Rev. B* **81**, 180405 (2010).

[8] Kim, M., Kim, B. H., Choi, H. C., and Min, B. I. *Phys. Rev. B* **81**, 100409 (2010).

[9] Nandy, A. K., Mahadevan, P., Sen, P., and Sarma, D. D. *Phys. Rev. Lett.* **105**, 056403 (2010).

[10] Appleyard, E. T. S. and Lovell, A. C. B. *Proc. Roy. Soc. Lon. A Math. Phys. Sci.* **158**, 718 (1937).

[11] Lovell, A. C. B. *Proc. Roy. Soc. Lon. A Math. Phys. Sci.* **166**, 270 (1938).

[12] Wu, J. X., Ma, M. S., Liu, X. M., Zhu, J. S., Ji, M. R., Xu, P. S., and Zhao, T. X. *Phys. Rev. B* **51**, 14286 (1995).

[13] Zhu, J. S., Wu, J. X., Liu, X. M., Mas, M. S., and Ji, M. R. *Surf. Sci.* **389**, 1 (1997).

[14] Shek, M. L., Pan, X. H., Strongin, M., and Ruckman, M. W. *Phys. Rev. B* **34**, 3741 (1986).

[15] Hrbek, J., Yang, Y. W., and Rodriguez, J. A. *Surf. Sci.* **296**, 164 (1993).

[16] Moulder, J. F., Stickle, W. F., Sobol, P. E., and Bomben, K. D. *Handbook of X-ray Photoelectron Spectroscopy.* Physical Electronics Inc., (1995).

[17] Qiu, S. L., Lin, C. L., Chen, J., and Strongin, M. *Phys. Rev. B* **41**, 7467 (1990).

[18] Qiu, S. L., Lin, C. L., Chen, J., and Strongin, M. *J. Vac. Sci. Technol. A* **8**, 2595 (1990).

[19] Wu, J. X., Liu, X. M., Ma, M. S., Bai, M., Ji, M. R., and Zhu, J. S. *Appl. Surf. Sci.* **153**, 150 (2000).

[20] Bagus, P. S., Pacchioni, G., Sousa, C., Minerva, T., and Parmigiani, F. *Chem. Phys. Lett.* **196**, 641 (1992).

[21] Joannis, M. A. *Compt. Rend.* **116**, 1370 (1893).

[22] Rengade, E. *Ann. Chim. Phys.* **140**, 1536 (1905).

[23] Rengade, E. *Ann. Chim. Phys.* **11**, 348 (1907).

[24] Vannerberg, N. *Prog. Inorg. Chem.* **4**, 125 (1962).

[25] Kunze, N. and Oetken, M. *Chemkon* **17**, 7 (2010).

[26] Thomas, L. C. *Interpreting Unexpected Events and Transitions in DSC Results.* TA Instruments Inc.